PHYSICS

Unconditional Fock state generation using arbitrarily weak photonic nonlinearities

Andrew Lingenfelter[1,2]*, David Roberts[1,2], A. A. Clerk[1]

We present a mechanism that harnesses extremely weak Kerr-type nonlinearities in a single driven cavity to deterministically generate single-photon Fock states and more general photon-blockaded states. Our method is effective even for nonlinearities that are orders-of-magnitude smaller than photonic loss. It is also completely distinct from so-called unconventional photon blockade mechanisms, as the generated states are non-Gaussian, exhibit a sharp cutoff in their photon number distribution, and can be arbitrarily close to a single-photon Fock state. Our ideas require only standard linear and parametric drives and are hence compatible with a variety of different photonic platforms.

INTRODUCTION

Single-photon Fock states are a fundamental resource needed in a myriad of quantum information protocols and technologies. There is as a result enormous interest in resource-friendly methods for their production (*1*). A generic, well-studied mechanism is photon blockade (*2*): Apply a monochromatic drive to a nonlinear photonic cavity such that the drive is only resonant for the vacuum to one photon transition but not for higher transitions. While conceptually simple, this conventional photon blockade (CPB) mechanism requires the single-photon nonlinearity to be much larger than the loss rate. This regime can be achieved in highly nonlinear cavities incorporating single atoms (*3*), quantum dots (*4*), or superconducting qubits (*5*, *6*). Unfortunately, this standard type of photon blockade is completely out of reach in more conventional systems that exhibit only weak nonlinearities (e.g., optical micro- or nanoresonators fabricated using materials with intrinsic $\chi^{(3)}$ nonlinearities).

The ability to realize effects akin to photon blockade in weakly nonlinear systems would be an incredibly powerful resource. There has thus been a flurry of theoretical activity to uncover possible such mechanisms. Among the best known proposals is that of "unconventional photon blockade" (UPB), where states with arbitrarily small $g^{(2)}(0)$ correlation functions can be generated using extremely weak nonlinearities. UPB was originally proposed in (*7*) and subsequently analyzed in many different works (*8*–*17*). It has also been realized experimentally in a circuit quantum electrodynamics (QED) platform (*18*) and in a quantum dot plus cavity setup (*19*). Unfortunately, UPB is only capable of generating Gaussian states that have positive-definite Wigner functions and that do not exhibit a true cutoff in their photon number distribution (*11*); moreover, they only exhibit suppressed intensity fluctuations in the limit where the average photon number is vanishingly small. These features severely limit their utility for many possible applications. We note that an alternative approach to stabilizing intracavity Fock states is to use dissipation-engineering ideas [see, e.g., (*20*–*23*)]. These methods are, however, also resource demanding and require strong, structured nonlinearities.

In this work, we propose and analyze a previously unidentified photon blockade mechanism that (unlike UPB) deterministically generates truly non-Gaussian blockaded states (i.e., zero probability for more than one photon) using arbitrarily weak single-photon nonlinearities (see Fig. 1). In further contrast to UPB, this can be achieved while also having the single-Fock state probability to be order 1. Our mechanism is based on using nonlinearity to modify matrix elements of an effective cavity driving process, as opposed to introducing nonlinearity in a spectrum (as is done in CPB), see Fig. 2. In its simplest form, it reduces to realizing an effective single-mode Hamiltonian of the form

$$\hat{H}_{\text{block}} = \widetilde{\Lambda}_3 \hat{a}^\dagger(\hat{a}^\dagger\hat{a} - r) + \text{h.c.} \tag{1}$$

where the parameter r is tuned to 1. h.c., hermitian conjugate. Here, $\hat{a}$ is the cavity annihilation operator and $\widetilde{\Lambda}_3$ is the amplitude of an effective nonlinear driving process. By construction, this Hamiltonian connects the vacuum and one photon states but does not allow driving from $|1\rangle$ to the $|2\rangle$ photon state. Crucially, as this blockade is a matrix element effect, it is effective even if cavity loss is much larger than the nonlinearity $\widetilde{\Lambda}_3$.

While the basic mechanism in Eq. 1 is extremely simple, it describes an unusual nonlinear driving element. At first glance, it is not at all obvious how to realize this Hamiltonian using standard $\chi^{(2)}$ or $\chi^{(3)}$ type optical nonlinearities. Despite its exotic form, we show that it can be achieved using standard ingredients: a standard Kerr-type nonlinearity (strength U), along with standard single-photon and two-photon (i.e., parametric) drives. Crucially, the mechanism is effective even if the Kerr nonlinearity strength U is much weaker than the cavity loss rate κ. We also discuss how our scheme can be realized using three-wave mixing type (i.e., $\chi^{(2)}$) nonlinearities.

In what follows, we analyze in detail the physics of our basic mechanism and how it could be harnessed for a time-dependent protocol that generates propagating Fock states in a variety of realistic weakly nonlinear optical setups. We also discuss extensions of our basic idea, where the same underlying mechanism can be used to generate more complex blockaded states and even multimode non-Gaussian entangled states (see the Supplementary Materials). Note that the infinite-time, steady-state properties of a damped cavity subject to the driving in Eq. 1 (in a displaced frame) were studied in (*24*). While this steady state could be tuned to realize a partial blockade effect, the effect was extremely limited. The steady state never exhibited Wigner-function negativity and, moreover, was exponentially fragile to imperfections (i.e., a small

[1]Pritzker School of Molecular Engineering, University of Chicago, Chicago, IL 60637, USA. [2]Department of Physics, University of Chicago, Chicago, IL 60637, USA.
*Corresponding author. Email: lingenfelter@uchicago.edu

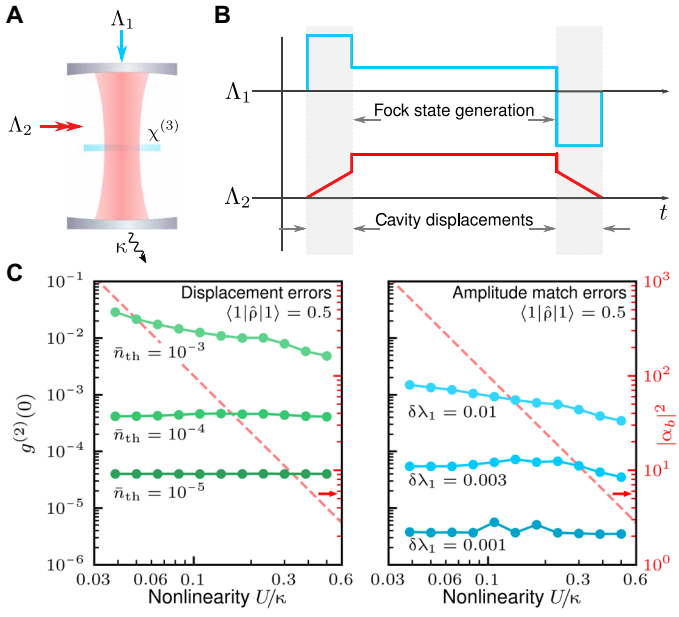

Fig. 1. Fock states with ultraweak nonlinearities. (**A**) Basic system: A nonlinear cavity is subject to both one- and two-photon drives Λ_1 and Λ_2. (**B**) Time dependence of drive amplitudes for the protocol (see the "Generating single-photon states in the laboratory frame" section). The key idea is to realize an effective nonlinear one-photon drive in a displaced frame. (**C**) Numerical simulations of performance including imperfections. Parameters are chosen such that the effective nonlinear drive amplitude $\widetilde{\Lambda}_3 = 2\kappa$ and the final state has $\langle 1|\hat{\rho}|1\rangle = 0.5$. Left: $g^{(2)}(0)$ of the prepared state including errors in the initial/final displacement operations; these are modeled as added thermal noise ($\bar{n}_{\mathrm{th}}$ quanta). Note that with added thermal noise, $g^{(2)}(0)$ must be greater than $\bar{n}_{\mathrm{th}}$. Right: Final $g^{(2)}(0)$ with imperfect drive-amplitude matching $\delta\lambda_1 \neq 0$ (cf. Eq. 7). Red dashed lines show intracavity photon number $|\alpha_b|^2 \sim (\kappa/U)^2$ during the intermediate part of the protocol.

deviation of the parameter r from an integer value completely destroyed the partial blockade). The utility of this effect was thus marginal. In contrast, our work here explores the finite-time dynamics of systems with this kind of nonlinear driving. We show that, unexpectedly, our model exhibits metastability and two distinct slow relaxation time scales. The intermediate-time physics can thus be extremely different from the ultimate steady state. In particular, this regime enables the near-perfect generation of Fock states (including states with highly negative Wigner functions) in a way that is robust against imperfections. We also stress that (*24*) did not discuss or analyze a concrete implementation of Eq. 1 in a generic driven Kerr cavity system or did it analyze an explicit time-dependent Fock state generation protocol; it also did not identify, let alone describe, quantitatively the unexpected long-lived metastability of this system. These are all crucial and new features of our work.

RESULTS

Basic mechanism and realization in a driven, weakly nonlinear cavity

Despite wanting to realize a somewhat exotic nonlinear drive (cf. Eq. 1), we will consider a physical system that is both conventional and ubiquitous. It consists of a single mode of a bosonic resonator (frequency ω_c, lowering operator $\hat{a}$) having a weak self-Kerr nonlinearity U, which is subject to both one- and two-photon drives

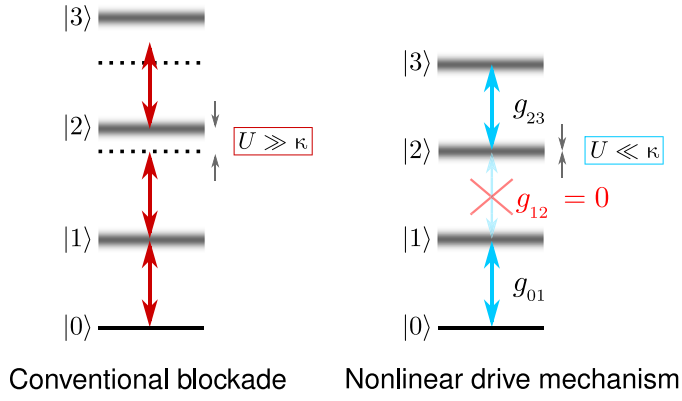

Fig. 2. Basic photon blockade mechanisms. Left: CPB mechanisms rely on the nonlinearity U shifting the spectrum of the system; blockade thus requires $U \gg \kappa$. Right: Our new approach is based on engineering a nonlinear drive that has no matrix element g_{12} connecting Fock states $|1\rangle$ and $|2\rangle$. This blockade mechanism is effective even if nonlinearity is arbitrarily weak.

with amplitudes Λ_1 and Λ_2, respectively, and commensurate drive frequencies $2\omega_1 = \omega_2$. Starting from the laboratory-frame Hamiltonian, moving to the rotating frame set by ω_1, and making a standard rotating wave approximation (RWA), we find (see Materials and Methods)

$$\hat{H}_{\mathrm{RWA}} = U\hat{a}^\dagger\hat{a}^\dagger\hat{a}\hat{a} + \Delta\hat{a}^\dagger\hat{a} + (\Lambda_1\hat{a}^\dagger + \Lambda_2\hat{a}^\dagger\hat{a}^\dagger + \mathrm{h.c.}) \quad (2)$$

Here, $\Delta = \omega_c - \omega_1$ is the detuning of the drives from cavity resonance. We stress that the two-photon drive Λ_2 can be realized in many different ways. For example, one could use a weak nonlinear coupling to a strongly pumped auxiliary mode or just simply apply two additional (linear) drive tones to the main cavity mode [see, e.g., (*25*)]. Our results below do not depend on the specific method of implementation.

From a quantum optics perspective, our driven cavity mode seems innocuous: It has an extremely weak Kerr nonlinearity and simple quadratic driving terms (which on their own would only generate simple Gaussian states). To obtain something more interesting, our general approach is to use linear driving (i.e., a displacement in phase space) to effectively enhance the effects of U. Such linear displacements are often used to enhance the properties of weakly nonlinear systems by yielding tuneable linear dynamics (e.g., parametric amplifiers realized by driving weakly nonlinear cavities or tuneable sideband interactions in quantum optomechanics (*26*)). Such linear dynamics does not allow for the generation of nonclassical, non-Gaussian states. Here, we show how a displacement can be used to generate an effective nonlinear cavity drive with a strength $\gg U$. We note that linear driving has also been used in circuit QED experiments to generate a tuneable longitudinal coupling between a qubit and a cavity (*27*–*29*). The interaction in those works is a single-photon cavity drive whose phase is controlled by an auxiliary qubit. This is distinct from the kind of interaction we realize, namely, a single-photon cavity drive whose magnitude is controlled by the photon number of the cavity itself, as opposed to that of a highly nonlinear auxiliary system.

We show that by moving to a displaced frame of the cavity, $\hat{a} \to \hat{a} + \alpha$, where α is an arbitrary displacement parameter, we can generate a displacement-enhanced nonlinearity that is precisely the

term we seek to engineer (see Materials and Methods). Upon moving to a displaced frame of the cavity, we find that the Kerr nonlinearity generates, among corrections to the other terms in $\hat{H}_{\mathrm{RWA}}$, the desired nonlinear drive $\widetilde{\Lambda}_3\,\hat{a}^\dagger\hat{a}^\dagger\hat{a}$ + h.c. with drive amplitude $\widetilde{\Lambda}_3 = 2U\alpha$ (see Materials and Methods, Eq. 15d).

Our goal is to realize (in our displaced frame) the ideal blockade Hamiltonian

$$\hat{H}_{\mathrm{target}} = (\widetilde{\Lambda}_3\,\hat{a}^\dagger(\hat{a}^\dagger\hat{a} - r) + \mathrm{h.c.}) + U\hat{a}^\dagger\hat{a}^\dagger\hat{a}\hat{a} \tag{3}$$

To achieve this, we first decide on a desired strength for the nonlinear drive amplitude $\widetilde{\Lambda}_3$ in $\hat{H}_{\mathrm{target}}$ and pick the displacement parameter α to achieve this. This requires

$$\alpha \to \alpha_b \equiv \frac{\widetilde{\Lambda}_3}{2U} \tag{4}$$

We will typically want $\widetilde{\Lambda}_3 \gtrsim \kappa$, implying that a large displacement will be needed if the nonlinearity U is weak.

The last step is to pick our original drive parameters Λ_1, Λ_2, and Δ to make the remaining terms in the full displaced Hamiltonian $\hat{H}_\alpha$ (see Eq. 14 in Materials and Methods) match $\hat{H}_{\mathrm{target}}$. This leads to the choices

$$\Lambda_1 \to \Lambda_{1,b} \equiv \widetilde{\Lambda}_3\left[-r + \frac{|\widetilde{\Lambda}_3|^2}{2U^2} + \frac{i\kappa}{4U}\right] \tag{5a}$$

$$\Lambda_2 \to \Lambda_{2,b} \equiv -\widetilde{\Lambda}_3^2/4U \tag{5b}$$

$$\Delta \to \Delta_b \equiv -|\widetilde{\Lambda}_3|^2/U \tag{5c}$$

With this choice of drive parameters and displacement parameter α, our displaced-frame Hamiltonian $\hat{H}_\alpha$ has exactly the desired form of the target blockade-producing Hamiltonian in Eq. 3. If we pick r in Eq. 5a to be an integer, it follows that we can achieve blockaded dynamics in the displaced frame. To be concrete, imagine we tune parameters to achieve $r = 1$. If we then start the system in the vacuum of the displaced frame (i.e., a coherent state in the lab frame), then the full system dynamics will be confined to the Fock states $n = 0$, $n = 1$ in the displaced frame, regardless of how small the original value of U was.

We have thus demonstrated how the basic physics of Eq. 1 can be realized using an arbitrarily weak Kerr nonlinearity and standard one- and two-photon driving processes. Note that the magnitude of the nonlinear driving in the displaced frame is the product of the original Kerr nonlinearity U (which could be extremely small) and the displacement α (which at this stage, we can assume to be very large). There is, of course, an important caveat about our scheme at this stage: As described, it only yields blockaded states and Fock states in the displaced frame. As we show in the "Generating single-photon states in the laboratory frame" section below, this is not a true limitation, as we can easily harness this physics to generate true laboratory-frame Fock states (see also Fig. 1).

Blockade dynamics in the presence of loss

Before addressing how one converts displaced-frame blockaded states into truly blockaded states, we first investigate the dynamics of our system in the displaced frame. We thus study displaced-frame master equation

$$\frac{d}{dt}\hat{\rho} = -i[\hat{H}_{\mathrm{target}}, \hat{\rho}] + \kappa\mathcal{D}[\hat{a}]\hat{\rho} \tag{6}$$

where $\hat{H}_{\mathrm{target}}$ is given by Eq. 3. We will consider the dynamics when the parameter r is close to, but not identical, to its ideal value for an $n = 1$ Fock state blockade, i.e., $r = 1 + \delta r$. In practice, δr corresponds to a failure to exactly match the one- and two-photon drive amplitudes in the ideal required manner, as dictated by Eqs. 5a and 5b. Our focus here will be primarily on understanding the temporal dynamics on time scales $t \lesssim 1/\kappa$ and using this to identify optimal parameters for generating Fock states.

Dynamics for ideal drive amplitude matching

For perfect parameter tuning $\delta r = 0$, we have ideal blockade dynamics where the drive cannot connect the $n = 1$ and $n = 2$ Fock states. Within the blockade manifold spanned by $\{|0\rangle, |1\rangle\}$, the cavity behaves like a two-level-system, which is resonantly driven with Rabi frequency $\propto \widetilde{\Lambda}_3$, i.e., $\hat{H}_{\mathrm{target}} \to \widetilde{\Lambda}_3|1\rangle\langle 0| + \mathrm{h.c.}$ As there is no probability of having two or more photons, for this perfect tuning of r, the equal-time $g^{(2)}$ correlation function [defined as $g^{(2)}(0) \equiv \langle\hat{a}^\dagger\hat{a}^\dagger\hat{a}\hat{a}\rangle/\langle\hat{a}^\dagger\hat{a}\rangle^2$] is always exactly 0. To generate a single-photon state, we simply need to perform an effective π-pulse. This amounts to turning on the one- and two- photon drives [with the ideal amplitudes given by Eqs. 5a and 5b for a time $t_\pi = \pi/(2|\widetilde{\Lambda}_3|)$. This allows the perfect generation of a Fock state in the limit where $t_\pi \ll 1/\kappa$, requiring $|\widetilde{\Lambda}_3|/\kappa \gg 1$. We stress that this condition can be met even if $U \ll \kappa$.

Impact of imperfect drive-amplitude matching

We now consider what is likely the dominant error mechanism for our scheme: the inability to perfectly match the drive amplitudes Λ_1 and Λ_2 as required to achieve $r = 1$. For small mismatch δr, there is only a weak matrix element connecting $|1\rangle$ to $|2\rangle$. As we will show, this means that we still have approximate blockade physics over a long time scale, enabling the production of nonclassical blockaded states. The perfect single photon blockade we desire requires matching the linear and cubic driving terms in the displaced-frame Hamiltonian $\hat{H}_\alpha$ (cf. Eq. 14), i.e., $\widetilde{\Lambda}_1 = -\widetilde{\Lambda}_3$ (i.e., $r = 1$). Deviations from this amplitude-matching condition will then degrade our scheme. We thus define $\delta\lambda_1$, the dimensionless relative amplitude error in the single-photon drive amplitude, via

$$\widetilde{\Lambda}_1 = -\widetilde{\Lambda}_3(1 + \delta\lambda_1) \tag{7}$$

While, in general, both the magnitude and phase of $\delta\lambda_1$ are important, for the small deviations we focus on here, only the magnitude matters. We take $\delta\lambda_1$ real and positive for all of the numerical simulations.

To get some analytic insight into the impact of this imperfection, consider the most interesting regime of small imperfection $|\delta\lambda_1| \ll 1$ and large effective driving, $|\widetilde{\Lambda}_3| > \kappa$. For short times, dissipation can be neglected, and further, the dynamics will be restricted to the states $|0\rangle$, $|1\rangle$, and $|2\rangle$ (as the leakage to higher levels is weak). In this regime, we find that the instantaneous $g^{(2)}(0; t)$ is time independent and given by

$$g^{(2)}(0; t) = |\delta\lambda_1|^2 \tag{8}$$

This suggests that highly blockaded states are possible without requiring an incredibly precise balancing of drive amplitudes.

In Fig. 3 (B and C), we show the results of a numerical simulation of the effects of a nonzero drive-amplitude mismatch $\delta\lambda_1$. We see that the intracavity average photon number shown in Fig. 3B undergoes Rabi oscillations before leaving the blockaded subspace; we also see that Eq. 8 provides a good description of the intracavity $g^{(2)}(0)$ until a time $t \sim 1/|\widetilde{\Lambda}_3|$, after which there is a departure from the blockaded subspace. The net result of our simulations and analysis is that errors in amplitude matching do not prevent the generation of useful blockaded states: For short times, the evolution produces states with small $g^{(2)}(0)$ while, at the same time, having appreciable nonvacuum population. As Fig. 3 shows, even for relative mismatches of $\delta\lambda_1 \sim 0.1$, blockaded states with $\langle \hat{a}^\dagger \hat{a} \rangle \sim 0.5$ and $g^{(2)}(0) < 0.1$ can be produced.

Slow time scales, metastability, and blockaded states in the infinite-time limit

While for applications, the relatively robust blockade physics we obtain at short times is more than sufficient, it is also interesting to ask about the nature of the long-time steady state. For $\delta\lambda_1 = 0$, the blockade is perfect for all times, and the steady state has no population of higher Fock states. With imperfections, the situation is different. We saw above that the short-time blockade physics is relatively robust against amplitude mismatch errors. This, however, is not true for the infinite-time state. As discussed in Materials and Methods, for $\delta\lambda_1 = 0$, the system has a long-lived, metastable high-photon number state that is only able to decay via quantum tunneling. This manifests itself as an extremely slow relaxation rate (i.e., dissipative gap)

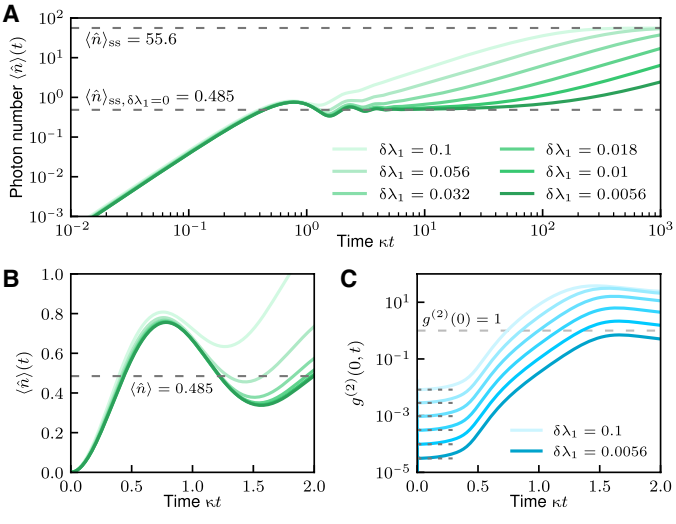

Fig. 3. Impact of mismatched drive amplitudes on blockade dynamics. (**A**) Average intracavity photon number versus time (log axes) for values of the dimensionless relative amplitude mismatch $\delta\lambda_1$ (cf. Eq. 7). One clearly sees two distinct time scales: The desired low-amplitude blockaded state is reached on a time scale $\sim 1/\kappa$, whereas if $\delta\lambda_1 \neq 0$, then there is a much slower heating to a high amplitude state, Γ_{esc} (cf. Eq. 10). Note that all of the $\delta\lambda_1$ shown are much larger than the "antiresonance" width Δr for these parameters (cf. Fig. 6), i.e., the steady-state blockade is destroyed for all $\delta\lambda_1$ shown. (**B**) Zoom-in on short-time behavior of (A), linear axes. The dashed curve is the ideal $\delta\lambda_1 = 0$ steady-state average photon number. (**C**) Instantaneous intracavity correlation function $g^{(2)}(0; t)$, for various imperfection levels $\delta\lambda_1$. Dashed lines correspond to the short-time analytic result in Eq. 8. For all plots, we use parameters $U = 0.4\kappa$ and $\widetilde{\Lambda}_3 = 2\kappa$.

$$\gamma_{slow} \sim \kappa \exp\left(-\frac{9\,|\widetilde{\Lambda}_3|^2}{4U^2}\right) \tag{9}$$

(cf. Eq. 23 and preceding discussion in Materials and Methods). This exponentially small dissipative gap directly leads to the extreme fragility of the steady-state photon blockade to even minuscule mismatches of drive amplitude. A simple perturbative argument suggests that the steady state blockade is lost when $|\delta\lambda_1| \simeq \gamma_{slow}/\kappa$, i.e., even when $|\delta\lambda_1| \ll 1$ (cf. "Photon blockade in the infinite-time steady state" in Materials and Methods). This fragility makes the steady-state effect essentially unattainable in experiment. Note that the extreme sensitivity of the steady state to relative drive amplitudes was first observed without explanation in (*24*); the qualitative and quantitative explanations of this phenomenon provided in Materials and Methods is, however, new to this work.

One might worry that this small dissipative gap should also have made the finite-time blockade physics presented above highly fragile. This is not the case: For an imperfect system that starts from vacuum, there is a distinct metastable regime of relevance whose physics is controlled by a different time scale unrelated to $1/\gamma_{slow}$. The relevant rate Γ_{esc} now corresponds to a slow escape from the blockaded subspace. For imperfect amplitude matching ($\delta\lambda_1 \neq 0$), there is a weak coupling between blockaded and unblockaded subspaces. Once in the unblockaded subspace, the system can eventually populate the weakly metastable, high-amplitude state. While this escape destroys the blockade and results in a very large average photon number in the steady state, this corruption occurs over a very slow time scale $1/\Gamma_{esc}$. The slow heating associated with this phenomena can be seen in Fig. 3A.

The escape rate Γ_{esc} can be estimated using a Fermi's Golden Rule (FGR) argument where $\delta\lambda_1$ (the imperfection in the single-photon drive amplitude) is treated as a perturbation. This is consistent with the numerically observed behavior that the average intracavity photon number approaches its steady-state value exponentially. Defining $\delta\widetilde{\Lambda}_1 = \widetilde{\Lambda}_3 \times \delta\lambda_1$, an approximate FGR calculation yields (see Materials and Methods)

$$\Gamma_{esc} = c\,\frac{|\delta\widetilde{\Lambda}_1|^2}{\kappa} \tag{10}$$

with c is a dimensionless number. While, in general, it will depend on other parameters in the unperturbed Hamiltonian, for $\kappa \gg \widetilde{\Lambda}_3$, we find that it is constant: $c = 1$. In contrast, for the regime of interest $\kappa \sim \widetilde{\Lambda}_3$, a simple analytic estimate is not possible. We do, however, find from numerics in this regime (i.e., by fitting the long-time relaxation of the average photon number shown in Fig. 3A) that $c \approx 0.25$ in this regime. The overall form of Γ_{esc} reflects two basic facts: The cavity can only leave the blockade subspace through the very small matrix element $\propto \delta\widetilde{\Lambda}_1$, and the cavity must jump into energy eigenstates, which are not localized to the Fock state $|2\rangle$ but spread out in Fock space and thus harder to jump into. The latter effect leads generically to $c < 1$.

The slow escape rate Γ_{esc} defines a time window over which the blockaded subspace is isolated from the rest of Hilbert space. To prepare Fock states, one just needs this time to be long compared to inverse drive amplitudes. In practice, this leads to the weak constraint on drive-amplitude matching $\delta\lambda_1 < 1$. This is to be contrasted against the exponentially more demanding condition needed for blockade physics in the steady state, $\delta\lambda_1 < \gamma_{slow}/\kappa$. The vast difference

in these conditions means that our blockade mechanism is with reach of various experimental platforms, whereas in contrast, the steady-state version of the effect is completely impractical.

Photon blockade with weak drive

The short-time blockade physics we have considered so far requires $\widetilde{\Lambda}_3 > \kappa$. Via Eq. 4, we see that this is possible even if $U \ll \kappa$, as long as we use a large displacement α_b. While at a fundamental level, such large displacements pose no problems, but at a practical level, they can create issues. We will see this explicitly in the next section, where we discuss in detail how to turn the displaced-frame Fock states produced by Eq. 3 to true laboratory-frame Fock states.

Given this possible concern, it is also interesting to ask about the dynamics of system where $|\widetilde{\Lambda}_3| \ll \kappa$, a regime that could be reached with small U and modest displacements α. Consider first the case where the drive amplitudes are perfectly matched, implying $r = 1$ in Eq. 3. In this case, the system approaches the infinite-time, perfectly blockaded steady state on a time scale $\sim 1/\kappa$. This state has zero probability for having more than one photon, and the single photon occupancy is

$$\langle 1|\hat{\rho}(t \to \infty)|1\rangle = \frac{4|\widetilde{\Lambda}_3/\kappa|^2}{1+8|\widetilde{\Lambda}_3/\kappa|^2} \tag{11}$$

Hence, having a weak $\widetilde{\Lambda}_3/\kappa$ does not break the blockade but just reduces the population of the one photon state. On the bright side, in this weak drive regime, the blockade much more robust to amplitude mismatch errors. Figure 4A shows the transition from the underdamped regime $\widetilde{\Lambda}_3 > \kappa/4$, where coherent oscillations are visible, to the overdamped regime where the cavity exponentially relaxes to the steady state. The robustness of the overdamped blockade is shown in Fig. 4A where the $g^{(2)}(0; t)$ of the overdamped blockade remains near the amplitude-mismatch–limited value $g^{(2)}(0; t) = |\delta\lambda_1|^2$ given by Eq. 8 for long times even as the underdamped blockade experiences a large rise in $g^{(2)}(0; t)$ for times $\kappa t \sim 1$.

Generating single-photon states in the laboratory frame

Our discussion so far has established how, using a cavity mode with an extremely weak Kerr nonlinearity $U \ll \kappa$ and standard one- and two-photon drives, it is possible to generate truly photon-blockaded states in a displaced frame. In the displaced frame and for ideal matching of drive amplitudes, these states have zero population of states with two or more photons and, moreover, can have a population of the $|1\rangle$ Fock state that approaches one. We also showed that this physics is robust, again modest errors in matching the two drive amplitudes appropriately.

We discussed the displacement transformation $\hat{a} \to \hat{a} + \alpha$ that led to the Hamiltonian in Eq. 14 as a passive transformation. To make use of this idea to generate true Fock states, we now view the displacement as an active transformation: A short, high-amplitude one-photon drive will be used to initially and rapidly displace the cavity state by an amplitude α_b. A similar protocol will then be used to undo this displacement at the end of the blockade protocol. In what follows, we discuss each step of this protocol in detail, including a treatment of error mechanisms associated with imperfect displacements.

Protocol overview

The basic idea of the full scheme is sketched in Fig. 5. It has three main steps:

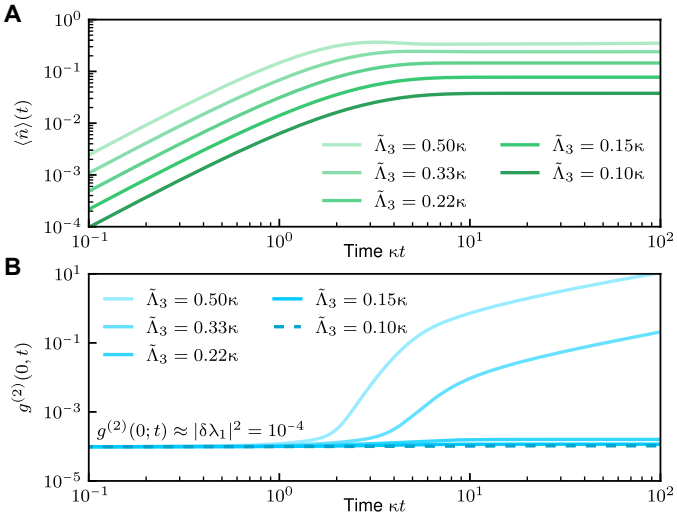

Fig. 4. Photon blockade dynamics with weak $\widetilde{\Lambda}_3$ drive. As discussed in the text, the resource requirements of our scheme are greatly reduced if one only tries to achieve a nonlinear drive $\widetilde{\Lambda}_3 \lesssim \kappa$. (**A**) Average intracavity photon number versus time for an imperfect drive amplitude matching $\delta\lambda_1 = 0.01$, for different $\widetilde{\Lambda}_3$. As expected, $\langle \hat{n} \rangle$ (t) approaches its steady state value (cf. Eq. 11) in a time $\sim 1/\kappa$. Reducing $\widetilde{\Lambda}_3$ reduces this value. (**B**) Instantaneous intracavity $g^{(2)}(0; t)$ of the cavity as a function of time, with $\delta\lambda_1 = 0.01$. Even for modest drives $\widetilde{\Lambda}_3 < \kappa$, a good blockade is achieved at short times. For all plots, $U = 0.075\kappa$.

1) Initial displacement: With the cavity initially in vacuum $|0\rangle$, we rapidly displace the cavity (using the one-photon drive) to the coherent state $|\alpha_b\rangle$ (see Eq. 4).

2) Fock state generation: We next turn on the two-photon drive and set both the drive amplitudes Λ_1 and Λ_2 to their ideal values given by Eqs. 5a and 5b. We then let the system evolve for an optimally chosen time $\tau_{\text{block}} \sim |\widetilde{\Lambda}_3|^{-1}$. This will prepare to good approximation a single-photon blockaded state in the displaced frame.

3) Final displacement: Last, we turn off the two-photon drive and adjust the amplitude of the one-photon drive Λ_1 such that rapidly displaces the cavity by an amount $-\alpha_b$. This then shifts our displaced-frame blockaded state to laboratory-frame blockaded state (ideally the state $|1\rangle$).

The end result of the three steps above is a blockaded, approximate single-photon state in the cavity. To turn this into a more useful propagating single-photon state, we imagine a situation where the cavity is overcoupled to a waveguide or transmission line. In this case, one simple waits at the end of step three. The intracavity state will then preferentially leak out into waveguide as an approximate Fock state in a propagating mode with an exponential profile. Note that while overcoupling will increase κ, this is not overly detrimental to our protocol. As we have stressed, our protocol can be effective even if the Kerr nonlinearity U is much smaller than the total loss rate κ of the cavity.

The initial and final displacements in our protocol are of course key aspects needed to achieve our final, laboratory-frame photon-blockaded state. As discussed, these should correspond to amplitudes α_b and $-\alpha_b$ respectively, where this amplitude is determined by Eq. 4. A failure to perform this ideally represents another possible experimental imperfection that would degrade from our scheme. Even if the one-photon drive used to perform these displacements

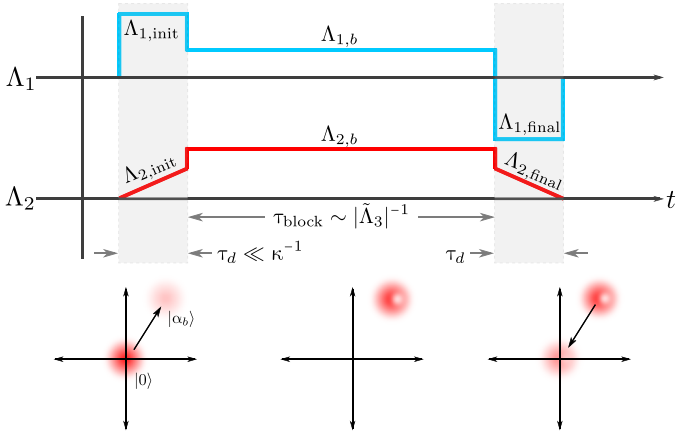

Fig. 5. Fock state generation protocol timing diagram. Top: Three steps of the generation protocol described in the "Protocol overview" section. The gray regions are the initial and final cavity displacements, which are implemented by applying strong one photon drives (Λ_1) to the cavity for a short displacement time $\tau_d \ll \kappa^{-1}$. Ramped two-photon drives (Λ_2) are also applied to correct unwanted squeezing generated by U during these displacement operations. The white region represents the displaced-frame Fock state generation step; here, one- and two-photon drive amplitudes are tuned to their ideal values as given by Eqs. 5a to 5c. The evolution here occurs for a duration $\tau_{\mathrm{block}} \sim |\tilde{\Lambda}_3|^{-1}$ that can be optimized, during which the cavity evolves under Eq. 13. Bottom: Cavity phase space diagram showing schematically the evolution of the cavity state in the laboratory frame.

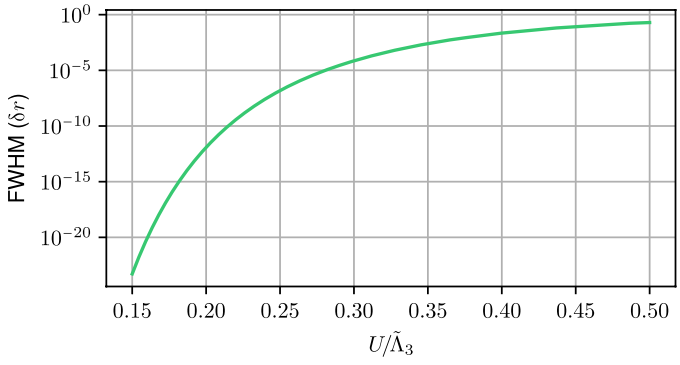

Fig. 6. Steady state photon number antiresonance width as a function of $U/\tilde{\Lambda}_3$. Full width at half maximum (FWHM) of the steady-state photon number at the single-photon blockade antiresonance as a function of $U/\tilde{\Lambda}_3$ as measured by the small deviation $\delta\lambda_1$ (cf. Eq. 7).

can be calibrated perfectly, the weak cavity nonlinearity U can cause errors during steps 1 and 3 of the protocol. The dominant error is an unwanted parametric drive generated via U; this could be canceled by also applying a compensating two-photon drive $\Lambda_2 \neq 0$ during steps 1 and 3; this is depicted in Fig. 5. In what follows, as opposed to focusing on a particular mechanism, we use a general model to characterize errors in the displacement steps (steps 1 and 3) of our general protocol.

Numerical results

Having outlined our full protocol, we numerically study its performance. Step 2 is modeled exactly, by evolving our system as per the full master equation in Eq. 13. The possibly imperfect displacement operations in steps 1 and 3 are modeled as a combination of a perfect displacement and the injection of thermal noise (corresponding to $\bar{n}_{\mathrm{th}}$ thermal quanta). Formally, this corresponds to a Gaussian additive noise channel (*30*). Note that this additive thermal noise rapidly degrades the blockade. If we start with a perfect Fock state $|1\rangle$ and add $\bar{n}_{\mathrm{th}}$ thermal quanta (via an additive Gaussian noise channel), then one can show that $g^{(2)}(0) \geq 4\bar{n}_{\mathrm{th}}$. Further details are provided in the Supplementary Materials, as are results for limitations arising from classical displacement and phase noise.

In addition to displacement errors, we consider drive amplitude mismatches, which we discussed in the "Impact of imperfect drive-amplitude matching" section. The results of that analysis apply here, but as a check, we perform the full Fock state generation protocol with small $\delta\lambda_1 \neq 0$. The figure of merit for the Fock state generation protocol is the instantaneous second-order coherence $g^{(2)}(0)$ at the end of the protocol as a function of U/κ.

Numerical simulations of our full time-dependent protocol for various choices of U/κ are shown in Fig. 1C. In each case, parameters are chosen to produce (in the ideal case) a state where the blockaded state has $\langle 1|\hat{\rho}|1\rangle = 0.5$. The numerical results show that the blockade protocol is effective even for $U/\kappa = 0.03$ and, moreover, is robust against both small displacement errors and small amplitude match errors. There is no fundamental limit against applying our protocol for even smaller values of U. Numerics becomes somewhat unwieldy, given the large displacements $\alpha_b \sim \kappa/U$ that are required.

DISCUSSION

A key virtue of our scheme is that it is extremely generic: There are many different kinds of systems that can realize weakly nonlinear electromagnetic modes with one- and two-photon drives. In the context of weakly nonlinear optical cavities, the primary experimental challenge for implementation is the large cavity displacements required, $\alpha_b \sim \kappa/U$. For typical low-loss silicon microresonators, the intrinsic $\chi^{(3)}$ nonlinearity yields $U/\kappa \sim 10^{-8}$ (*31*). The $\chi^{(3)}$ of silicon nitride is typically even smaller (*32*–*34*). While the large displacements and intracavity powers required in such systems to achieve $\alpha_b \sim \kappa/U$ may be possible given the pulsed nature of our scheme, a safer route would be to follow the general ideas in the "Photon blockade with weak drive" section. Here, one uses displacements much smaller than κ/U, making constraints on power handling much more reasonable. This results in a perfect blockade and states with vanishingly small $g^{(2)}(0)$. The price to pay, however, is that the average photon number will also be very small. We stress that even in this regime, the states generated have a strong advantage over the UPB mechanism of (*7*): Unlike UPB, our states are non-Gaussian and have zero population of higher Fock states.

An alternative route for implementation in optical cavities would be to use $\chi^{(2)}$ nonlinearities in materials with broken inversion symmetry like silicon nitride or aluminum nitride. These nonlinearities are parametrically larger than the corresponding $\chi^{(3)}$; a recent experiment even achieved a single-photon $\chi^{(2)}$ nonlinearity that was $\sim 0.01\kappa$ (*35*). We stress that while our scheme requires a Kerr-type four-wave mixing nonlinearity, this can be achieved starting with three-wave mixing $\chi^{(2)}$ processes that generate a nonlinear coupling to a detuned auxiliary mode (*36*). To the second order in this coupling, one generates the desired self-Kerr interaction U needed

for our scheme. Despite being the second order, this can still be orders-of-magnitude larger than an intrinsic $\chi^{(3)}$ nonlinearity.

While optical cavities are one possible domain of application, they are not the only candidate. Our ideas could also be exploited in parametrically driven nanomechanical systems with weak intrinsic Duffing nonlinearities [see, e.g., (*37*)], as well as in microwave cavity systems. A current trend in quantum information processing with superconducting circuits is to store and process information in high-Q microwave cavities [see, e.g., (*38*, *39*)]. In such schemes, detuned qubits are often used to induce weak nonlinearities in the principle bosonic modes. A key limitation in these approaches is that the qubit also induces additional loss mechanisms. Our ideas here suggest a path to circumvent this. One could use extremely large qubit-cavity detunings, resulting in not only very weak induced cavity nonlinearities but also weak induced dissipation. Our scheme shows that such weak nonlinearities could still be harnessed to produce nonclassical states.

In this work, we have described a previously unidentified basic route to generating photonic states that are blockaded: They have a sharp cutoff in their photon number distribution, having zero probability to have more than r photons in the state. This is accomplished by using standard tools (a weak Kerr nonlinearity, one- and two-photon drives) to realize an effective nonlinear drive, cf. Eq. 3. In stark contrast to the well-studied UPB mechanism (*7*), our scheme can generate truly blockaded states and states that do not need to be infinitely close to being vacuum. In principle, our basic mechanism is effective even for arbitrarily weak nonlinearities $U \ll \kappa$. In practice, limitations will arise from the inability to perfectly match the one- and two-photon drive amplitudes and the inability to apply the required displacement transformations perfectly. We showed that the scheme nonetheless can be effective even if these imperfections are present.

While our analysis focused on generating states that approximate single-photon Fock states, the idea is much more general. By picking the parameter r in Eq. 3 to be an integer larger than one (which then influences the choice of drive amplitudes via Eqs. 5a and 5b), one can generate higher-order blockaded states: states that are confined to the manifold spanned by Fock states $|0\rangle, |1\rangle, \ldots, |r\rangle$. Further, the same basic idea can used to generate nonclassical, multimode entangled states. One again realizes the nonlinear driving Hamiltonian in Eq. 3 in a displaced frame, but now the mode $\hat{a}$ is actually a collective mode of two or more distinct cavity modes. Generating a Fock state in this collective mode directly corresponds to a W-style entangled state. More details are provided in the Supplementary Materials.

In summary, we believe that the mechanism discussed here will prove to be valuable tool for generating nonclassical photonic states in a variety of platforms where only weak nonlinearities are achievable. It could also conceivably be harnessed as a tool for quantum simulation, i.e., to realize models of strongly interacting photons. Our ideas are compatible with a wide variety of bosonic systems, including optical and microwave cavities, as well as more general superconducting circuit QED setups.

MATERIALS AND METHODS

RWA Hamiltonian

A crucial result of this work is that to implement the nonlinear photon drive of Eq. 1, we require only a single mode of a bosonic resonator with a weak self-Kerr nonlinearity U and standard one- and two-photon drives. The starting laboratory-frame Hamiltonian is thus ($\hbar = 1$)

$$\begin{aligned}\widehat{H} &= \omega_c \hat{a}^\dagger \hat{a} + \frac{U}{6}(\hat{a} + \hat{a}^\dagger)^4 \\ &+ (\Lambda_1 e^{-i\omega_1 t} + \Lambda_1^* e^{i\omega_1 t})(\hat{a} + \hat{a}^\dagger) \\ &+ (\Lambda_2 e^{-i\omega_2 t} + \Lambda_2^* e^{i\omega_2 t})(\hat{a}\hat{a} + \hat{a}^\dagger \hat{a}^\dagger)\end{aligned} \tag{12}$$

Note that the only nonlinearity in this Hamiltonian is Kerr interaction U, which we will allow to be extremely weak, i.e., $U \ll \kappa$, where κ is the cavity loss rate. The two-photon drive Λ_2 is a standard parametric drive and can be realized without requiring a strong single-photon nonlinearity.

We choose the drive frequencies to satisfy $\omega_2 = 2\omega_1 = 2(\omega_c - \Delta)$, implying that they are equally detuned from the resonance by an amount Δ. We also work in the standard regime where ω_c is the largest frequency in the problem, allowing us to make an RWA on both the nonlinearity and drive terms. Making the RWA and working in the rotating frame set by the drive frequency ω_1, we obtain Eq. 2. Note that we have normal-ordered the nonlinearity; thus, the nonlinearity strength in $\widehat{H}_{\mathrm{RWA}}$ is U. Note also that normal-ordering shifts the resonance to $\widetilde{\omega}_c = \omega_c + 2U$; we implicitly assume the detuning from resonance in $\widehat{H}_{\mathrm{RWA}}$ is thus $\Delta = \omega_1 - \widetilde{\omega}_c$.

Displacement transformation

We use strong driving to enhance the effects of U in $\widehat{H}_{\mathrm{RWA}}$. We also include single-photon loss at a rate κ using a standard Lindblad master equation description. Letting $\hat{\rho}$ denote the reduced density matrix of the cavity mode, we have

$$\frac{d}{dt}\hat{\rho} = -i[\widehat{H}_{\mathrm{RWA}}, \hat{\rho}] + \kappa \mathcal{D}[\hat{a}]\hat{\rho} \tag{13}$$

where $\mathcal{D}[\hat{a}]\widehat{O} = (\hat{a}\widehat{O}\hat{a}^\dagger - \{\hat{a}^\dagger \hat{a}, \widehat{O}\}/2)$ is the standard Lindblad dissipative superoperator.

The trick is now to show that with appropriate parameter tuning, a simple displacement of our weakly nonlinear Hamiltonian in Eq. 2 can yield exactly the kind of nonlinear driving interaction we are looking for. In particular, we want a Hamiltonian that is unitarily equivalent to $\widehat{H}_{\mathrm{target}}$ in Eq. 3, where the parameter r will be set to a positive integer. This Hamiltonian describes a nonlinear driving process that can pump up an initial vacuum state to the $n = r$ Fock state but no higher.

To achieve this equivalence, we consider a displacement transformation to a new frame where the original photonic vacuum is shifted to the coherent state $|-\alpha\rangle$; we leave the amplitude α unspecified for the moment. This required unitary is $\mathcal{D}_\alpha = \exp(\alpha \hat{a}^\dagger - \alpha^* \hat{a})$, which transforms the lowering operator as $\hat{a} \to \hat{a} + \alpha$. In this new displaced frame, the master equation for our system has the same form as Eq. 13 but with a modified displaced Hamiltonian $\widehat{H}_\alpha$

$$\begin{aligned}\widehat{H}_\alpha &= U\hat{a}^\dagger \hat{a}^\dagger \hat{a}\hat{a} + \widetilde{\Delta}\hat{a}^\dagger \hat{a} \\ &+ (\widetilde{\Lambda}_1 \hat{a}^\dagger + \widetilde{\Lambda}_2 \hat{a}^\dagger \hat{a}^\dagger + \widetilde{\Lambda}_3 \hat{a}^\dagger \hat{a}^\dagger \hat{a} + \mathrm{h.c.})\end{aligned} \tag{14}$$

All of the terms in the original laboratory-frame Hamiltonian appear in $\widehat{H}_\alpha$ but with altered coefficients; we also generate the desired nonlinear single-photon driving term $\widetilde{\Lambda}_3$. The displaced-frame Hamiltonian parameters are

$$\widetilde{\Delta} = \Delta + 4U|\alpha|^2 \tag{15a}$$

$$\widetilde{\Lambda}_1 = \Lambda_1 + \alpha\Delta + 2\alpha^*\Lambda_2 + 2U|\alpha|^2\alpha - \frac{1}{2}i\kappa\alpha \tag{15b}$$

$$\widetilde{\Lambda}_2 = \Lambda_2 + U\alpha^2 \tag{15c}$$

$$\widetilde{\Lambda}_3 = 2U\alpha \tag{15d}$$

Notice that by picking the displacement α and the laboratory-frame Hamiltonian parameters Λ_1, Λ_2, and Δ, we have complete control over all of the displaced-frame Hamiltonian parameters. In particular, the choices in Eqs. 4 and 5 lead to the target Hamiltonian $\widehat{H}_{\text{target}}$. In addition, notice that the displacement transformation modifies the Lindblad dissipator as $\mathcal{D}[\hat{a}] \mapsto \mathcal{D}[\hat{a} + \alpha]$, which we rewrite as $\mathcal{D}[\hat{a}] - i[(-i\alpha\kappa/2)\hat{a}^\dagger + \text{h.c.}, \rho]$. The induced coherent linear drive component has been absorbed into $\widetilde{\Lambda}_1$ in Eq. 13b. The net result is that the damping rate of the cavity is the same in the displaced frame.

Photon blockade in the infinite-time steady state

The main focus of our work is understanding Fock state generation using the dynamics of Eq. 13 for times much shorter than the full relaxation time of the system. Here, we comment on features of the infinite-time steady state. The properties of this steady state were discussed in (*24*) using an exact-solution technique.

As discussed, when r is exactly tuned to an integer, the steady state exhibits blockade: the steady state photon number distribution truncates at $n = r$. Unexpectedly, this blockade phenomenon is lost even for extremely small deviations of r away from an integer. This manifests itself as an antiresonance phenomenon when the average photon number in the steady state, $\langle\hat{n}\rangle_{\text{ss}}$ is plotted versus r. There is a sharp dip in this quantity when r is an integer, with the width of these features $\Delta r \ll 1$. This behavior is illustrated in Fig. 6, where we plot the full-width half-maximum Δr for the antiresonance in $\langle\hat{n}(r)\rangle_{\text{ss}}$ centered at $r = 1$. We plot this width as a function of $\widetilde{\Lambda}_3/U$. The plot shows an exponential dependence on this parameter. Away from the blockade point $r = 1$, the steady-state photon number is approximately constant and has a large value $\gg 1$.

Both the large average steady-state photon number away from integer r and the extremely small antiresonance widths can be understood starting with a semiclassical analysis, which reveals a large-amplitude metastable state. The semiclassical equation of motion for the amplitude $\alpha = \langle\hat{a}\rangle$ that follows from Eq. 13 is

$$\frac{d}{dt}\alpha = -2\text{i}U\alpha^*\alpha^2 - 2i\widetilde{\Lambda}_3\alpha^*\alpha - i\widetilde{\Lambda}_3\alpha^2 + i\widetilde{\Lambda}_3 r - \frac{\kappa}{2}\alpha \tag{16}$$

For $r = 0$ (nonlinear drive only) and $\kappa = 0$, the steady-state solutions to this equation are $\alpha_0 = 0$ (with multiplicity 2) and

$$\alpha_{\text{ha}} = -\frac{3\widetilde{\Lambda}_3}{2U} \tag{17}$$

Because we always assume a regime where $U \ll \widetilde{\Lambda}_3$, this amplitude is typically very large. Including nonzero κ and r, we find that the first-order correction to this amplitude is small. To the first order, we have

$$\alpha_{\text{ha}} = -\frac{3\widetilde{\Lambda}_3}{2U} - \frac{i\kappa}{2\widetilde{\Lambda}_3} + \frac{2U}{9\widetilde{\Lambda}_3}r \tag{18}$$

We can also confirm that this is an accurate description of the large-amplitude state by numerically finding the fixed points to Eq. 16 without assuming small r and κ.

Next, we show that this semiclassical solution is stable by performing a standard linear stability analysis of the semiclassical equations. The eigenvalues of the linearized equations of motion for α and α^* about α_{ha} are

$$\lambda_\pm = -\frac{\kappa}{2} \pm i3\sqrt{3}\frac{\widetilde{\Lambda}_3^2}{2U}\left(1 - \frac{8}{27}\frac{U^2}{\widetilde{\Lambda}_3^2}r\right) \tag{19}$$

which have negative real parts, indicating linear stability at the semiclassical level. Turning to the quantum problem, our system always has a unique steady state, which, for integer r, is a blockaded state. Hence, for integer r, the above semiclassically stable state is only unstable due to quantum effects (i.e., precisely the blockade physics we have described, which is intimately tied to the discreteness of photon number).

Returning to the quantum problem, we find that upon numerically diagonalizing $\widehat{H}_{\text{block}}$ in Eq. 1, there is an eigenstate $|\Phi\rangle$ with photon number $\langle\hat{n}\rangle_\Phi \approx |\alpha_{\text{ha}}|^2$ where α_{ha} is given by Eq. 19. Focusing on the single photon blockade, $r = 1$, we numerically diagonalize the Liouvillian Eq. 13, which reveals that there is generically a single nonzero eigenvalue γ_{slow}, which is significantly smaller than κ; all other decay rates are order κ or larger. We seek to show that this eigenvalue corresponds to the decay of the Hamiltonian eigenstate $|\Phi\rangle$ and that the value is exponentially small in $\widetilde{\Lambda}_3/U$.

Working under the assumption that $|\Phi\rangle$ is the state whose decay is given by the Liouvillian eigenvalue γ_{slow}, we use the first-order degenerate Liouvillian perturbation theory to estimate γ_{slow}. The exact eigenstates within the single photon blockade manifold $\{|0\rangle, |1\rangle\}$ are given by

$$|\psi_\pm\rangle = \frac{1}{\sqrt{2}}(|0\rangle \pm |1\rangle);\ E_\pm = \mp\widetilde{\Lambda}_3 \tag{20}$$

Note that these span the $\{|0\rangle, |1\rangle\}$ manifold so that $\langle 0|\Phi\rangle = \langle 1|\Phi\rangle = 0$. Using the numerically computed $|\Phi\rangle$, we find that it is reasonably well approximated by the coherent state $|\alpha_{\text{ha}}\rangle$ with overlap $|\langle\alpha_{\text{ha}}|\Phi\rangle|^2 > 0.96$ for $U \ll \widetilde{\Lambda}_3$. We enforce orthogonality with the blockade eigenstates (Eq. 20), which gives us the approximate eigenstate

$$|\phi\rangle = \frac{1}{\mathcal{N}}(|\alpha_{\text{ha}}\rangle - e^{-\frac{1}{2}|\alpha_{\text{ha}}|^2}|0\rangle - \alpha_{\text{ha}}e^{-\frac{1}{2}|\alpha_{\text{ha}}|^2}|1\rangle) \tag{21}$$

where $\mathcal{N}$ is the normalization constant. Under the assumption that $|\phi\rangle$ is an approximate eigenstate of $\widehat{H}_{\text{block}}$, the relevant three-eigenstate degenerate manifold of the unperturbed Liouvillian $\mathcal{L}_0 = -i[\widehat{H}_{\text{block}}, \cdot]$ is $\{|\psi_+\rangle\langle\psi_+|, |\psi_-\rangle\langle\psi_-|, |\phi\rangle\langle\phi|\}$ (the third exact eigenstate is $|\Phi\rangle\langle\Phi|$ of course). The perturbation is single photon loss

$$\mathcal{L}_1 = \kappa\mathcal{D}[\hat{a}] \tag{22}$$

where $\mathcal{D}[\hat{X}]$ is the standard Lindblad dissipator. We diagonalize the three state subspace with respect to $\mathcal{L}_1$ and compute the eigenvalues. The irrelevant eigenvalues are $\gamma_0 = 0$, whose eigenvector is the $\kappa \ll \widetilde{\Lambda}_3$ limit of the single photon blockade steady state, and $\gamma_1 = \kappa/2$, whose eigenvector describes population imbalance relative

to the steady state. The final eigenvalue is the only one whose eigenvector involves $|\phi\rangle\langle\phi|$ and for $U \ll \widetilde{\Lambda}_3$ is given by

$$\gamma_{\text{slow}} \approx \kappa |\alpha_{\text{ha}}|^2 (1 + 2|\alpha_{\text{ha}}|^2) e^{-|\alpha_{\text{ha}}|^2} \tag{23}$$

This shows that the dissipative gap of the blockade Liouvillian spectrum is exponentially small in $U/\widetilde{\Lambda}_3 \ll 1$ due to a quasistable eigenstate of the coherent Hamiltonian. We thus have provided a quantitative and intuitive understandingof the unexpected sensitivity of the steady state to small deviations of r away from integer values, explaining the unexpectedly sharp antiresonance phenomena found in (*24*).

Estimation of Γ_{esc}

We provide details here on how to use FGR to estimate the slow rate Γ_{esc} (c.f. Eq. 10), which governs escape from the blockaded subspace in the presence of imperfect drive amplitudes. Consider first the simple case where $\kappa \ll \widetilde{\Lambda}_3$. We write the system Hamiltonian $\widehat{H} = \widehat{H}_0 + (\delta\widetilde{\Lambda}_1 \hat{a}^\dagger + \text{h.c.})$, where $\widehat{H}_0$ is the ideal Hamiltonian with perfect drive amplitude matching (i.e., $\widehat{H}_0 = \widehat{H}_{\text{target}}$ with $r = 1$, c.f. Eq. 3). Treating the last term as a perturbation and letting $|\phi_j\rangle$ (E_j) denote eigenstates (eigenvalues) of $\widehat{H}_0$, application of FGR yields

$$\Gamma_{\text{esc}} = \sum_{j\in\{\text{unblock}\}} |\langle\phi_j|\delta\widetilde{\Lambda}_1\hat{a}^\dagger|\phi_\pm\rangle|^2 \frac{\gamma_j/2}{(\Delta E)^2 + \gamma_j^2/4} \tag{24}$$

Here, $|\phi_\pm\rangle$ are the two blockade-subspace eigenstates of $\widehat{H}_0$, and $\Delta E = E_j - E_\pm$. The last factor in Eq. 24 corresponds to the lifetime-broadened density of states of each unblockaded eigenstate; for weak κ, the decay rate $\gamma_j = \kappa\langle\phi_j|\hat{a}^\dagger\hat{a}|\phi_j\rangle$. This general form matches that of Eq. 10, with a prefactor c that in general depends on the unblockaded eigenstates of $\widehat{H}_0$ and hence $U/\widetilde{\Lambda}_3$. We find good agreement between Eq. 24 (computed from exact diagonalization) and the rate extracted from numerical simulations of the system dynamics for weak κ. As an example, we consider $\widetilde{\Lambda}_3 = 100\,\kappa$. For $U/\widetilde{\Lambda}_3 = 0.2$, the estimate is $c = 0.0051$ and the extracted value from the dynamics is $c = 0.0047$, and for $U/\widetilde{\Lambda}_3 = 0.3$, the estimate is $c = 0.0036$ and the extracted value is $c = 0.0045$. These are typical of this parameter regime. The small value of c here directly reflects the delocalization of the unblockaded eigenstates.

For more general regimes, it is trickier to directly apply FGR, as one can no longer treat the effects of κ by simply lifetime broadening each unperturbed eigenstate. For $\kappa \gg \widetilde{\Lambda}_3$, one can use the fact that the large dissipation will disrupt the formation of coherent eigenstates outside the blockaded subspace. In this case, we can estimate Γ_{esc} by considering a transition from either $|\phi_\pm\rangle$ to the Fock state $|2\rangle$, whose decay rate is simply 2κ. This leads to an approximate decay rate corresponding to Eq. 10 with parameter-independent constant $c = 1$. For the most relevant regime $\kappa \sim \widetilde{\Lambda}_3$, it is difficult to rigorously calculate the decay rate as neither κ nor the unblockaded coherent dynamics can be treated perturbatively. As discussed in the "Slow time scales, metastability, and blockaded states in the infinite-time limit" section, numerically a good agreement is found to the general form in Eq. 10 with $c \sim 0.25$. Heuristically, this is consistent with the results presented above; the slightly smaller value of c corresponds to the partial delocalization of unblockaded eigenstates.

SUPPLEMENTARY MATERIALS

Supplementary material for this article is available at https://science.org/doi/10.1126/sciadv.abj1916

REFERENCES AND NOTES

1. M. D. Eisaman, J. Fan, A. Migdall, S. V. Polyakov, Invited review article: Single-photon sources and detectors. *Rev. Sci. Instrum.* **82**, 071101 (2011).
2. A. Imamoğlu, H. Schmidt, G. Woods, M. Deutsch, Strongly interacting photons in a nonlinear cavity. *Phys. Rev. Lett.* **79**, 1467–1470 (1997).
3. K. M. Birnbaum, A. Boca, R. Miller, A. D. Boozer, T. E. Northup, H. J. Kimble, Photon blockade in an optical cavity with one trapped atom. *Nature* **436**, 87–90 (2005).
4. A. Faraon, I. Fushman, D. Englund, N. Stoltz, P. Petroff, J. Vuckovic, Coherent generation of non-classical light on a chip via photon-induced tunnelling and blockade. *Nat. Phys.* **4**, 859–863 (2008).
5. C. Lang, D. Bozyigit, C. Eichler, L. Steffen, J. M. Fink, A. A. Abdumalikov, M. Baur, S. Filipp, M. P. da Silva, A. Blais, A. Wallraff, Observation of resonant photon blockade at microwave frequencies using correlation function measurements. *Phys. Rev. Lett.* **106**, 243601 (2011).
6. J. M. Fink, A. Dombi, A. Vukics, A. Wallraff, P. Domokos, Observation of the photon-blockade breakdown phase transition. *Phys. Rev. X* **7**, 011012 (2017).
7. T. C. H. Liew, V. Savona, Single photons from coupled quantum modes. *Phys. Rev. Lett.* **104**, 183601 (2010).
8. M. Bamba, A. Imamoğlu, I. Carusotto, C. Ciuti, Origin of strong photon antibunching in weakly nonlinear photonic molecules. *Phys. Rev. A* **83**, 021802 (2011).
9. H. Flayac, V. Savona, Input-output theory of the unconventional photon blockade. *Phys. Rev. A* **88**, 033836 (2013).
10. D. Gerace, V. Savona, Unconventional photon blockade in doubly resonant microcavities with second-order nonlinearity. *Phys. Rev. A* **89**, 031803 (2014).
11. M.-A. Lemonde, N. Didier, A. A. Clerk, Antibunching and unconventional photon blockade with Gaussian squeezed states. *Phys. Rev. A* **90**, 063824 (2014).
12. Y. H. Zhou, H. Z. Shen, X. X. Yi, Unconventional photon blockade with second-order nonlinearity. *Phys. Rev. A* **92**, 023838 (2015).
13. H. Wang, X. Gu, Y.-x. Liu, A. Miranowicz, F. Nori, Tunable photon blockade in a hybrid system consisting of an optomechanical device coupled to a two-level system. *Phys. Rev. A* **92**, 033806 (2015).
14. X.-W. Xu, A.-X. Chen, Y.-x. Liu, Phonon blockade in a nanomechanical resonator resonantly coupled to a qubit. *Phys. Rev. A* **94**, 063853 (2016).
15. H. Flayac, V. Savona, Unconventional photon blockade. *Phys. Rev. A* **96**, 053810 (2017).
16. B. Sarma, A. K. Sarma, Unconventional photon blockade in three-mode optomechanics. *Phys. Rev. A* **98**, 013826 (2018).
17. K. Hou, C. J. Zhu, Y. P. Yang, G. S. Agarwal, Interfering pathways for photon blockade in cavity QED with one and two qubits. *Phys. Rev. A* **100**, 063817 (2019).
18. C. Vaneph, A. Morvan, G. Aiello, M. Féchant, M. Aprili, J. Gabelli, J. Estève, Observation of the unconventional photon blockade in the microwave domain. *Phys. Rev. Lett.* **121**, 043602 (2018).
19. H. Snijders, J. Frey, J. Norman, H. Flayac, V. Savona, A. Gossard, J. Bowers, M. van Exter, D. Bouwmeester, W. Löffler, Observation of the Unconventional Photon Blockade. *Phys. Rev. Lett.* **121**, 043601 (2018).
20. A. Sarlette, P. Rouchon, Robust open-loop stabilization of Fock states by time-varying quantum interactions* *This paper presents research results of the Belgian Network DYSCO (Dynamical Systems, Control, and Optimization), funded by the Interuniversity Attraction Poles Programme, initiated by the Belgian State, Science Policy Office. The authors were partially supported by the ANR, Projet Blanc EMAQS ANR-2011-BS01-017-01 and Projet C-QUID BLAN-3-139579. *IFAC Proc. Vol.* **45**, 208–213 (2012).
21. D. Mogilevtsev, A. Mikhalychev, V. S. Shchesnovich, N. Korolkova, Nonlinear dissipation can combat linear loss. *Phys. Rev. A* **87**, 063847 (2013).
22. E. Holland, B. Vlastakis, R. Heeres, M. Reagor, U. Vool, Z. Leghtas, L. Frunzio, G. Kirchmair, M. Devoret, M. Mirrahimi, R. Schoelkopf, Single-photon-resolved Cross-Kerr interaction for autonomous stabilization of photon-number states. *Phys. Rev. Lett.* **115**, 180501 (2015).
23. J.-R. Souquet, A. A. Clerk, Fock-state stabilization and emission in superconducting circuits using dc-biased Josephson junctions. *Phys. Rev. A* **93**, 060301 (2016).
24. D. Roberts, A. A. Clerk, Driven-dissipative quantum Kerr resonators: New exact solutions, photon blockade and quantum bistability. *Phys. Rev. X* **10**, 021022 (2020).
25. A. Kamal, A. Marblestone, M. Devoret, Signal-to-pump back action and self-oscillation in double-pump Josephson parametric amplifier. *Phys. Rev. B* **79**, 184301 (2009).
26. M. Aspelmeyer, T. J. Kippenberg, F. Marquardt, Cavity optomechanics. *Rev. Mod. Phys.* **86**, 1391–1452 (2014).
27. A. Eddins, S. Schreppler, D. Toyli, L. Martin, S. Hacohen-Gourgy, L. Govia, H. Ribeiro, A. Clerk, I. Siddiqi, Stroboscopic qubit measurement with squeezed illumination. *Phys. Rev. Lett.* **120**, 040505 (2018).
28. S. Touzard, A. Kou, N. E. Frattini, V. V. Sivak, S. Puri, A. Grimm, L. Frunzio, S. Shankar, M. H. Devoret, Gated conditional displacement readout of superconducting qubits. *Phys. Rev. Lett.* **122**, 080502 (2019).
29. P. Campagne-Ibarcq, A. Eickbusch, S. Touzard, E. Zalys-Geller, N. E. Frattini, V. V. Sivak, P. Reinhold, S. Puri, S. Shankar, R. J. Schoelkopf, L. Frunzio, M. Mirrahimi, M. H. Devoret,

Quantum error correction of a qubit encoded in grid states of an oscillator. *Nature* **584**, 368–372 (2020).
30. C. Weedbrook, S. Pirandola, R. García-Patrón, N. J. Cerf, T. C. Ralph, J. H. Shapiro, S. Lloyd, Gaussian quantum information. *Rev. Mod. Phys.* **84**, 621–669 (2012).
31. Z. Vernon, J. E. Sipe, Spontaneous four-wave mixing in lossy microring resonators. *Phys. Rev. A* **91**, 053802 (2015).
32. K. Ikeda, R. E. Saperstein, N. Alic, Y. Fainman, Thermal and Kerr nonlinear properties of plasma-deposited silicon nitride/silicon dioxide waveguides. *Opt. Express* **16**, 12987–12994 (2008).
33. Z. Ye, A. Fülöp, O. B. Helgason, P. A. Andrekson, V. Torres-Company, Low-loss high-Q silicon-rich silicon nitride microresonators for Kerr nonlinear optics. *Opt. Lett.* **44**, 3326–3329 (2019).
34. H. K. Tsang, Y. Liu, Nonlinear optical properties of silicon waveguides. *Semicond. Sci. Technol.* **23**, 064007 (2008).
35. J. Lu, M. Li, C.-L. Zou, A. A. Sayem, H. X. Tang, Toward 1% single-photon anharmonicity with periodically poled lithium niobate microring resonators. *Optica* **7**, 1654–1659 (2020).
36. X. Guo, C.-L. Zou, L. Jiang, H. X. Tang, All-optical control of linear and nonlinear energy transfer via the zeno effect. *Phys. Rev. Lett.* **120**, 203902 (2018).
37. J. S. Huber, G. Rastelli, M. J. Seitner, J. Kölbl, W. Belzig, M. I. Dykman, E. M. Weig, Spectral evidence of squeezing of a weakly damped driven nanomechanical mode. *Phys. Rev. X* **10**, 021066 (2020).
38. S. Puri, L. St-Jean, J. A. Gross, A. Grimm, N. E. Frattini, P. S. Iyer, A. Krishna, S. Touzard, L. Jiang, A. Blais, S. T. Flammia, S. M. Girvin, Bias-preserving gates with stabilized cat qubits. *Sci. Adv.* **6**, eaay5901 (2020).
39. A. Grimm, N. E. Frattini, S. Puri, S. O. Mundhada, S. Touzard, M. Mirrahimi, S. M. Girvin, S. Shankar, M. Devoret, Stabilization and operation of a Kerr-cat qubit. *Nat. Publ. Group* **584**, 205–209 (2020).

Acknowledgments: We are grateful to H. Tang of Yale University for conversations. **Funding:** This work was primarily supported by the University of Chicago Materials Research Science and Engineering Center, which is funded by the National Science Foundation under grant no. DMR-1420709. This work was also supported by the Air Force Office of Scientific Research MURI program, under grant no. FA9550-19-1-0399 and by the Army Research Office under grant W911-NF-19-1-0380. It was completed in part with resources provided by the University of Chicago's Research Computing Center. A.A.C. also acknowledges support from the Simons Foundation through a Simons Investigator award. **Author contributions:** A.L., D.R., and A.A.C. conceived the ideas. A.L. and A.A.C. developed the theory. A.L. performed the numerical simulations. A.L. and A.A.C. wrote the manuscript. A.L., D.R., and A.A.C. revised and edited the manuscript. **Competing interests:** The authors declare that they have no competing interests. **Data and materials availability:** All data needed to evaluate the conclusions in the paper are present in the paper and/or the Supplementary Materials.

Submitted 27 April 2021
Accepted 6 October 2021
Published 26 November 2021
10.1126/sciadv.abj1916